Journal of Theoretical and Computational Acoustics
2050026 (15 pages)

DOI: 10.1142/S2591728520500267

On the spherical expansion for calculating the sound radiated by a baffled circular piston

Jiaxin Zhong* and Xiaojun Qiu
Centre for Audio, Acoustics and Vibration,
Faculty of Engineering and Information Technology,
University of Technology Sydney
New South Wales 2007, Australia
**jiaxin.zhong@student.uts.edu.ac*

Received 3 August 2020
Revised 22 September 2020
Accepted 22 October 2020
Published 10 December 2020

An efficient and accurate method for calculating the sound radiated by a baffled circular rigid piston is using spherical harmonics, and the solution is a series containing the integral of spherical Bessel functions. The integral is usually calculated with the generalized hypergeometric functions in existing literatures, which shows poor convergence at middle and high frequencies due to the overflow and the loss of significant figures. A rigorous and closed form solution of the integral is derived in this paper based on the recurrence method, which is accurate in the whole frequency range and thousands of times faster than the existing methods. It is shown that the proposed method can be extended for the calculation of the sound radiated by a baffled piston and an unbaffled resilient disk with axisymmetric velocity and pressure profiles, respectively, and some baffled rotating sources where the velocity profile is asymmetric.

Keywords: Piston radiation; spherical expansion; spherical Bessel functions.

1. Introduction

The sound radiated by a baffled circular piston is calculated with Rayleigh integral, which is unsolvable in most cases.[1] The direct numerical integration of Rayleigh integral can be used to obtain the result while the calculation time and required memory size increase significantly with frequency.[2] The most efficient and rigorous calculation method currently available is decomposing the integral into a series of spherical harmonics where the angular and radial components are related to Legendre and spherical Bessel functions, respectively.[1,3]

The expression of the series is different in different regions, resulting in paraxial, inner, and outer expansions. The existing methods work fine for the paraxial and inner expansions, but the calculation of the outer expansion is rather time-consuming at middle and high frequencies which will be focused on in this paper.

The paraxial expansion is used when the distance between the field point and the radiation axis is less than the transducer radius. In this expansion, each term of the series is obtained with a finite step of recurrences.[1] It converges rapidly, but the coordinates of the field point and the transducer radius are coupled in the argument of special functions. Although the paraxial region covers the major energy of a sound beam at high frequencies, it is sometimes necessary to calculate the sound pressure in other regions. For example, the ultrasounds outside the paraxial region need to be taken into consideration, otherwise the prediction of audio sounds generated by nonlinear interactions of intensive ultrasounds would be inaccurate.[4,5]

The inner expansion is valid when the distance between the field point and the transducer center is less than the transducer radius. Although the inner expansion converges slowly, the field coordinates are uncoupled in the argument of special functions which means the radial and angular components can be calculated separately for a large number of field points.[1,3] To improve the convergence performance, a feasible technique is estimating the values of truncated terms of the series.[3] The inner expansion is not widely used because this region is small and it is also covered by the paraxial region.

For the field point in the outer region where the distance between the point and the transducer center is larger than transducer radius, the outer expansion needs to be used.[1,3] The widely used expression of the outer expansion is related to the generalized hypergeometric function (GHF).[1,3] Although it converges rapidly at low frequencies, its convergence performance is poor at middle and high frequencies because the GHF is an alternating series, the calculation involves subtractions between large numbers resulting in loss of significant figures, and the number of summation terms increases rapidly as the frequency increases. Therefore, the extended precision of float numbers in computers or other special techniques have to be used, resulting in an increase of computation complexity.[6,7] Besides, the GHF is difficult to analyze if further operations on the solution are required, such as integrals.[4,8] and derivatives.[9] with respect to the coordinates and the transducer radius.

In this paper, the outer expansion for Rayleigh integral is given and the integral over spherical Bessel functions is simplified rigorously into a closed form based on the recurrence method. Compared to the existing GHF method, Gauss-Legendre quadrature, and Bessel expansion method, the proposed expression is accurate and computationally efficient in the whole frequency range. It can also be extended to other scenarios such as a baffled piston, an unbaffled resilient disk with axisymmetric velocity and pressure profiles, and some baffled rotating sources where the velocity profile is asymmetric.

2. Methods

As shown in Fig. 1, the sound pressure radiated by a baffled circular rigid piston with a radius of a is calculated with Rayleigh integral.[1,10]

$$p(\mathbf{r}) = -\frac{\mathrm{j}\rho_0\omega v_0}{2\pi}\int_0^{2\pi}\int_0^{a}\frac{\mathrm{e}^{\mathrm{j}k|\mathbf{r}-\mathbf{r}_\mathrm{s}|}}{|\mathbf{r}-\mathbf{r}_\mathrm{s}|}\rho_\mathrm{s}\mathrm{d}\rho_\mathrm{s}\mathrm{d}\varphi_\mathrm{s}, \tag{1}$$

where j is the imaginary unit, ρ_0 is the air density, ω is the angular frequency, v_0 is the uniform velocity amplitude, k is the wavenumber and ρ_s and φ_s are the polar radial and azimuthal angular coordinates of a source point $\mathbf{r}_\mathrm{s} = (x_\mathrm{s}, y_\mathrm{s}, z_\mathrm{s})$ on the radiation surface with $z_\mathrm{s} = 0$, and $\mathbf{r} = (x, y, z)$ is the field point. The time dependence term $\mathrm{e}^{-\mathrm{j}\omega t}$ is omitted and t is the time.

To simplify Eq. (1), a spherical coordinate system (r, θ, φ) is established based on the rectangular one (x, y, z), where r, θ and φ are the radial distance, zenithal angle and azimuthal angle, respectively. The spherical coordinates of the source point $\mathbf{r}_\mathrm{s}$ are consequently $r_\mathrm{s}, \theta_\mathrm{s} = \pi/2$, and φ_s. The simplified expression is a series of angular and radial components which are different in different regions. The existing methods work fine for the paraxial and inner regions,[1,3] so this paper focuses on the outer region where $r > a$.

The outer expansion of Eq. (1) using spherical harmonics can be obtained in different ways[1,3] and a simpler derivation is presented in Appendix A.1, which is

$$p(\mathbf{r}) = \rho_0 c_0 v_0 \sum_{n=0}^{\infty}(-1)^n\frac{(4n+1)\Gamma\left(n+\frac{1}{2}\right)}{\sqrt{\pi}\Gamma(n+1)}\mathrm{P}_{2n}(\cos\theta)\mathrm{h}_{2n}(kr)\left[\int_0^{ka}\xi\mathrm{j}_{2n}(\xi)\mathrm{d}\xi\right], \tag{2}$$

where $\mathrm{j}_{2n}(\cdot)$ is the spherical Bessel function, $\mathrm{h}_{2n}(\cdot)$ is the spherical Hankel function of the first kind, $\mathrm{P}_{2n}(\cdot)$ is the Legendre polynomial and $\Gamma(\cdot)$ is the Gamma function. It has been shown that the calculation of Eq. (2) is highly efficient compared to Eq. (1) without loss of accuracy.[1,3]

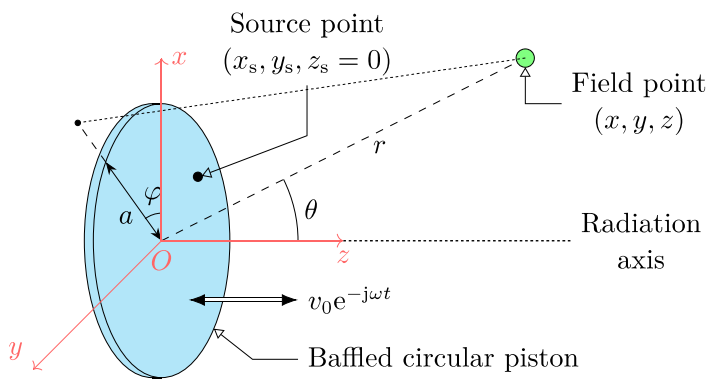

Fig. 1. Sketch of the radiation from a baffled circular rigid piston.

The integral in Eq. (2) is $\int_0^{ka} \xi \mathrm{j}_{2n}(\xi)\mathrm{d}\xi$ which is mostly calculated by the GHF ${}_1F_2(\cdot)$ in existing literatures.[1,3,8,9]

$$\int_0^{ka} \xi \mathrm{j}_{2n}(\xi)\mathrm{d}\xi = \sqrt{\pi}\left(\frac{ka}{2}\right)^{2n+2} \frac{\Gamma(n+1)}{\Gamma(n+2)\Gamma\left(n+\frac{3}{2}\right)} {}_1F_2\left(n+1; 2n+\frac{3}{2}, n+2; -\frac{(ka)^2}{4}\right). \tag{3}$$

Substituting the explicit expression of the GHF into Eq. (3) yields (denoted by "GHF series")

$$\int_0^{ka} \xi \mathrm{j}_{2n}(\xi)\mathrm{d}\xi = \sqrt{\pi}\left(\frac{ka}{2}\right)^{2n+2} \sum_{i=0}^{\infty} \frac{(-1)^i}{4^i(n+1+i)\Gamma\left(2n+\frac{3}{2}+i\right)} \frac{(ka)^{2i}}{i!}. \tag{4}$$

Equation (4) is usually calculated as the summation of truncated terms and converges rapidly when ka is small.[8] However, it shows poor convergence performance when ka is large (300 for example) for the following three reasons. First, it is an alternating series due to the factor $(-1)^i$; therefore, the calculation involves subtractions of large numbers when ka is large, resulting in a substantial loss of significant figures. Second, the number of summation terms required for a specified accuracy increases rapidly as ka increases, resulting in excessive computational load. Last, it easily leads to an arithmetic overflow for large ka before convergence because the terms in the summation are proportional to $(ka)^{2i}$.

To solve these problems, the extended precision of float numbers in computers and other special techniques have to be used to calculate GHFs with large arguments.[6,7] Some techniques have been adopted in MATLAB for the built-in function "hypergeom" to calculate GHFs numerically, but the calculation is still time-consuming and the obtained results are sometimes unreliable.[7] For example, when "hypergeom(1, 200, 1)" is called, the answers returned in MATLAB 2008b and MATLAB 2018a are different, which are 6.69×10^{299} and 1.005, respectively.[7] Furthermore, it is difficult for further operations on the expressions containing GHFs, which are necessary for some cases. For example, the derivative with respect to the disk radius, a, is used in Ref. 9 to obtain the radiation of a ring monopole source; the integral with respect to the radial coordinate of the field point, r, is used in Ref. 8 to obtain the sound generated from general radiator; and integrals with respect to both the radial and angular coordinates, r and θ, are used in Ref. 4 for the calculation of the audio sound generated by nonlinear interactions of intensive ultrasounds.

There are another two existing ways to calculate the integral in Eq. (3) numerically. One is using fundamental integration techniques such as the Gauss-Legendre quadrature (denoted by "Gauss-Legendre"), and the other is using infinite spherical Bessel function

expansion (Eq. (11.1.1) in Ref. 11; denoted by "Bessel expansion")

$$\int_0^{ka} \xi \mathrm{j}_{2n}(\xi)\mathrm{d}\xi = ka\frac{\Gamma(n+1)}{\Gamma\left(n+\frac{1}{2}\right)}\sum_{i=0}^{\infty}\left(2n+2i+\frac{3}{2}\right)\frac{\Gamma\left(n+i+\frac{1}{2}\right)}{\Gamma(n+i+2)}\mathrm{j}_{2n+2i+1}(ka). \tag{5}$$

Although these two methods work fine when n is comparable to or larger than ka, they also show poor convergence performance when n is smaller than ka because $\mathrm{j}_{2n}(\xi)$ oscillates significantly. For example, when $ka = 300$ and $n = 10$ as shown in the next section, more than 75 and 150 terms are required for these two methods, respectively, to reach satisfactory precisions. Furthermore, the required maximal terms of Gauss-Legendre quadrature and Bessel expansion are unclear for different orders n and arguments ka.

2.1. *Proposed closed form solution*

In following paragraphs, we will show that the integral can be rigorously simplified into a closed form so the sound pressure Eq. (2) can be calculated quickly and analytically. To simplify the derivation, an auxiliary indefinite integral is introduced as

$$\Phi_\nu^\mu(x) = \int x^\mu \mathrm{j}_\nu(x)\mathrm{d}x,\ \ \mu,\nu \in \mathrm{Z}. \tag{6}$$

Then the integrals in Eq. (2) are represented as $\Phi_{2n}^1(ka)$ and $\Phi_{2n}^1(0)$. For $n = 0$, the closed form of $\Phi_0^1(x) = -\cos x$ can be obtained by substituting the explicit expression of $\mathrm{j}_0(x) = \sin(x)/x$ into Eq. (6). For the case $n \geq 1$, it is hard to obtain the integral directly so the following recurrence relation is introduced:

$$\Phi_\nu^\mu(x) = (\nu+\mu-1)\Phi_{\nu-1}^{\mu-1}(x) - x^\mu \mathrm{j}_{\nu-1}(x), \tag{7}$$

which can be verified using the recurrence relation of spherical Bessel functions.[12] The recurrence steps for the calculation of $\Phi_{2n}^1(x)$ are

$$\begin{cases} \Phi_{2n}^1(x) = 2n\Phi_{2n-1}^0(x) - x\mathrm{j}_{2n-1}(x), & l = 0 \\ \Phi_{2n-1}^0(x) = 2(n-1)\Phi_{2n-2}^{-1}(x) - \mathrm{j}_{2n-2}(x), & l = 1 \\ \quad\vdots \qquad\qquad \vdots \qquad\qquad \vdots & \\ \Phi_{2n-l}^{1-l}(x) = 2(n-l)\Phi_{2n-l-1}^{-l}(x) - x^{1-l}\mathrm{j}_{2n-l-1}(x), & l \\ \quad\vdots \qquad\qquad \vdots \qquad\qquad \vdots & \\ \Phi_{n+1}^{2-n}(x) = 2\Phi_n^{1-n}(x) - x^{2-n}\mathrm{j}_n(x), & l = n-1 \\ \Phi_n^{1-n}(x) = 0 \times \Phi_{n-1}^{-n}(x) - x^{1-n}\mathrm{j}_{n-1}(x), & l = n, \end{cases} \tag{8}$$

which stop when $l = n$ because the coefficient of $\Phi_{n-1}^{-n}(x)$ becomes 0. Following the above relationships, $\Phi_{2n}^{1}(x)$ can be represented as

$$\Phi_{2n}^{1}(x) = -\sum_{l=0}^{n} 2^l \frac{\Gamma(n+1)}{\Gamma(n-l+1)} x^{1-l} \mathrm{j}_{2n-l-1}(x), \tag{9}$$

with $\Phi_{2n}^{1}(0) = -\sqrt{\pi}\Gamma(n+1)/\Gamma(n+\frac{1}{2})$.

Equation (9) is given in closed forms because $\mathrm{j}_{2n-l-1}(x)$ can be represented by a finite number of trigonometric functions, which are much easier to calculate than the GHF in Eq. (3), the Gauss-Legendre quadrature or the Bessel expansion in Eq. (5), especially when n is small and ka is large. For example, when $ka = 300$ and $n = 0$, Eq. (9) shows that only the calculation of the fundamental function $\mathrm{j}_{-1}(300) = \cos(300)/300$ is required to obtain the exact result. It is also noteworthy that no approximations are assumed in the derivation of Eq. (9), so it is accurate in the whole frequency range.

2.2. *Additional examples*

In addition to the rigid piston mentioned above, the proposed method can also be extended for other scenarios. When the velocity profile of the baffled circular piston is arbitrarily axisymmetric, it can be expanded into a summation of even-degree polynomials.[13,14] For example, for the velocity profile of the form $v_0[1-(\rho_\mathrm{s}/a)^{2m}], m = 0, 1, 2, \ldots$, the integral $\Phi_{2n}^{2m+1}(x)$ is required in the calculation of sound pressure and can be similarly obtained as (see Appendix A.1 for derivations)

$$\Phi_{2n}^{2m+1}(x) = -\sum_{l=0}^{n+m} 2^l \frac{\Gamma(n+m+1)}{\Gamma(n+m-l+1)} x^{2m-l+1} \mathrm{j}_{2n-l-1}(x), \tag{10}$$

with $\Phi_{2n}^{2m+1}(0) = -2^{2m}\sqrt{\pi}\Gamma(n+m+1)/\Gamma(n-m+\frac{1}{2})$.

When the pressure profile of a resilient disk in free space (without a baffle) is arbitrarily axisymmetric,[3,15] the integral $\Phi_{2n+1}^{2m}(x)$ is required and its closed form can be similarly obtained as (see Appendix A.2 for derivations)

$$\Phi_{2n+1}^{2m}(x) = -\sum_{l=0}^{n+m} 2^l \frac{\Gamma(n+m+1)}{\Gamma(n+m-l+1)} x^{2m-l} \mathrm{j}_{2n-l}(x), \tag{11}$$

with $\Phi_{2n+1}^{2m}(0) = -2^{2m-1}\sqrt{\pi}\Gamma(n+m+1)/\Gamma(n-m+\frac{3}{2})$.

In addition to the cases with axisymmetric profiles, the proposed method is also valid for some cases when the surface velocity or pressure profiles are asymmetric, such as the rotating source in an infinitely large baffle. In this case, the surface velocity profile at order ℓ can be given by $v(\rho_\mathrm{s})\cos(\ell\varphi_\mathrm{s})$, where the radial and angular components are separated and $\ell = 0$ corresponds to the axisymmetric case.[8] Here an example is presented, where $\ell = 1$, i.e. $v_0\rho_\mathrm{s}a^{-1}\cos(\varphi_\mathrm{s})$, representing the wobbling effects of a piston.[16] The spherical

expansions of the sound pressure can be expressed as (see Appendix A.3 for derivations)

$$p_{\mathrm{w}}(\mathbf{r}) = \frac{\rho_0 c_0 v_0}{ka}\cos\varphi \sum_{n=0}^{\infty}(-1)^{n+1}\frac{(4n+3)\Gamma\left(n+\frac{3}{2}\right)}{\sqrt{\pi}(2n+1)\Gamma(n+2)} \times \mathrm{P}^1_{2n+1}(\cos\theta)\mathrm{h}_{2n+1}(kr)\left[\int_0^{ka}\xi^2\mathrm{j}_{2n+1}(\xi)\mathrm{d}\xi\right], \tag{12}$$

where $\mathrm{P}^1_{2n+1}(\cdot)$ is the associated Legendre function at order 1 and the integral of $\Phi^2_{2n+1}(x) = \int x^2\mathrm{j}_{2n+1}(x)\mathrm{d}x$ can be obtained by the closed form given in Eq. (11).

3. Results and Discussions

The efficiency of the proposed method Eq. (9) for calculating the integral $\int_0^{ka}\xi\mathrm{j}_{2n}(\xi)\mathrm{d}\xi$ is firstly demonstrated by comparing the numerical results with the ones obtained by using the Gauss-Legendre quadrature, Bessel expansion Eq. (5), and the GHF series Eq. (4). Figure 2 shows the results of the integral obtained with the four methods at different ka and n. The abscissa represents the number of truncated terms in the Bessel expansion and GHF series, or the terms in the Gauss-Legendre quadrature, or the summation steps in the proposed solution.

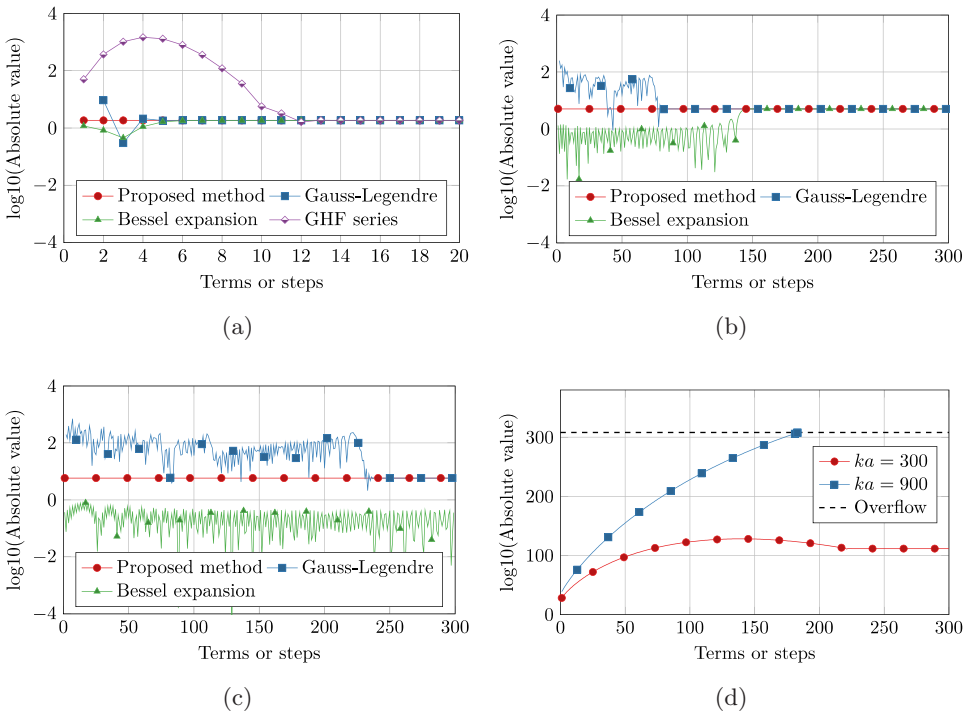

Fig. 2. Numerical calculation of the integral $\int_0^{ka}\xi\mathrm{j}_{2n}(\xi)\mathrm{d}\xi$ using four methods when (a) $ka = 10$ and $n = 0$; (b) $ka = 300$ and $n = 10$; (c) $ka = 900$ and $n = 10$ and (d) using the GHF series at $n = 10$.

It can be found in Fig. 2(a) that all the results converge rapidly when $ka = 10$, which is in the low-frequency range. However, the spherical Bessel functions oscillate significantly at large ka, so more terms are required in the Gauss-Legendre quadrature and Bessel expansion to obtain accurate results, such as more than 75 and 200 for Gauss-Legendre quadrature in Figs. 2(b) and 2(c), respectively. However, only 10 steps are required while using the proposed solution. When the frequency is high, e.g. $ka = 300$ or 900, the curve for the GHF series is not included in Figs. 2(b) and 2(c) because the results exceed the vertical axis range. These curves are plotted separately in Fig. 2(d) with larger vertical axis ranges. The first term of the GHF series of Eq. (4) is up to 10^{28} and 10^{38} for $ka = 300$ and 900, respectively, while the accurate results of the integral are only 5.05 and 5.84, respectively. The result for $ka = 900$ overflows when the truncated terms exceed 183, and the curve for $ka = 300$ converges to an incorrect result much larger than 5.84 due to the loss of significant figures as discussed in Sec. 2.

The GHF can also be calculated using the built-in function "hypergeom" in MATLAB where better but not publicly known techniques are used to solve the problems occurred in the direct summation of truncated terms of the GHF series Eq. (4). Table 1 compares the calculation time using the GHF calculated by this built-in function and the proposed method for the orders 0 to N, where N is the maximal order required for calculating the sound pressure in Eq. (2) to give satisfactory precisions. The calculation time using the GHF method increases as the ka and N increase and is more than 60 s when $ka = 900$ and $N = 600$, while the time with the proposed method is less than 0.1 s for all cases. Furthermore, it is noteworthy that the values calculated by MATLAB are sometimes unreliable and efforts should be spent to validate the accuracy case by case.[7]

In the following simulations, the common parameters used in modelling audio sounds generated by nonlinear interactions of intensive ultrasounds, i.e. a parametric array loudspeaker,[5] are used to verify the accuracy of the proposed solution. The radius of the transducer $a = 0.3$ m, the frequency $f = 65$ kHz, the complex wavenumber $k = \omega/c_0 + \mathrm{j}\alpha$, and $ka = 350 + 0.09\mathrm{j}$, where the sound speed $c_0 = 343$ m/s and the sound attenuation coefficient in air $\alpha = 0.3$ Neper/m, which is calculated according to ISO $9613 - 1$ at the temperature of 25°C and the relative humidity of 70%.[17]

Table 1. Comparison of the calculation time when the GHF is calculated by the built-in function "hypergeom" of MATLAB R2018a (based on a personal computer with 2.5GHz main frequency) and the proposed method.

Case	Calculation time (s)	
	GHF method	Proposed method
$ka = 300$, $N = 200$	9.47	0.0048
$ka = 500$, $N = 350$	23.12	0.016
$ka = 900$, $N = 600$	62.75	0.043

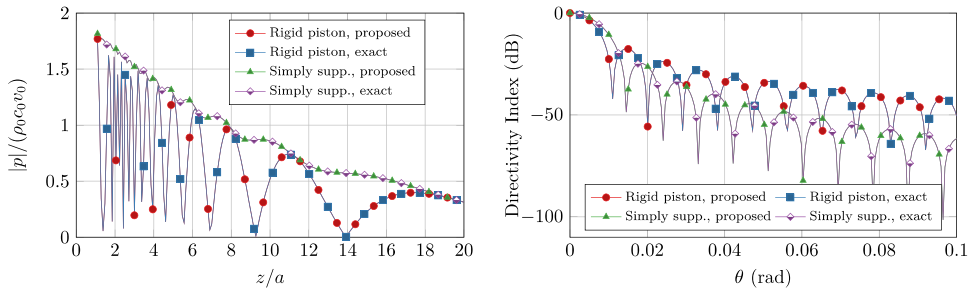

(a) (b)

Fig. 3. Calculated normalized sound pressure on the radiation axis (a) and the directivity index (b) when $ka = 350 + 0.09\mathrm{j}$ for a baffled circular radiator with the uniform (rigid piston) and quadratic (simply supported disk) velocity profiles.

Figure 3 shows the sound pressure on the radiation axis of the transducer and the directivity index, which is defined as $20\log_{10}[|p(\theta)/p(\theta=0)|]$ at $kr \to \infty$, for the surface velocity profile of the piston (v_0) and the simply supported disk ($2v_0[1-(\rho_s/a)^2]$).[14] In the proposed method, the on-axis pressure is calculated by Eq. (2) by setting $\theta = 0$, the directivity index is calculated by Eq. (2) after using the far field asymptotic formula $\mathrm{h}_{2n}(kr) \sim (-1)^n \mathrm{h}_0(kr)$ at $kr \to \infty$,

$$p(\mathbf{r}) = \rho_0 c_0 v_0 \mathrm{h}_0(kr) \sum_{n=0}^{\infty} \frac{(4n+1)\Gamma\left(n+\frac{1}{2}\right)}{\sqrt{\pi}\Gamma(n+1)} \mathrm{P}_{2n}(\cos\theta) \left[\int_0^{ka} \xi \mathrm{j}_{2n}(\xi)\mathrm{d}\xi\right], \quad kr \to \infty \tag{13}$$

and the number of truncated terms is set as 200. The exact values of the on-axis pressure and the directivity index are presented for comparison, which are calculated with Eqs. (20)–(29) in Ref. 14, respectively. The results obtained with the proposed method agree well with those from the exact solutions. This validates the accuracy of the proposed method in the outer region, where no closed form exact solution is available at present.

4. Conclusions

An outer expansion is derived for the sound radiation from a baffled circular rigid piston based on the recurrence relation of spherical Bessel functions. Unlike the existing GHF method, the Gauss-Legendre quadrature, and the infinite Bessel expansion, the expression is given in a closed form and can be calculated exactly with finite terms in the whole frequency range. In the proposed expression, the spherical coordinates of the field point and the disk radius are uncoupled, which is convenient for obtaining derivatives and integrals with respect to these parameters. The proposed method can also be extended to other scenarios, such as the radiation from a baffled circular piston with axisymmetric velocity profiles, a resilient disk in free space, and a baffled rotating source. Future work is to investigate the simplification of the sound radiated by a rectangular radiator.

Acknowledgment

This research is supported under the Australian Research Council's Linkage Project funding scheme (LP160100616).

References

1. T. D. Mast and F. Yu, Simplified expansions for radiation from a baffled circular piston, *J. Acoust. Soc. Am.* **118**(6) (2005) 3457–3464.
2. J. Zemanek, Beam behavior within the nearfield of a vibrating piston, *J. Acoust. Soc. Am.* **49**(1B) (1971) 181–191.
3. M. A. Poletti, Spherical expansions of sound radiation from resilient and rigid disks with reduced error, *J. Acoust. Soc. Am.* **144**(3) (2018) 1180–1189.
4. M. Červenka and M. Bednařík, Non-paraxial model for a parametric acoustic array, *J. Acoust. Soc. Am.* **134**(2) (2013) 933–938.
5. J. Zhong, R. Kirby, and X. Qiu, A spherical expansion for audio sounds generated by a circular parametric array loudspeaker, *J. Acoust. Soc. Am.* **147**(5) (2020) 3502–3510.
6. W. F. Perger, A. Bhalla and M. Nardin, A numerical evaluator for the generalized hypergeometric series, *Comput. Phys. Commun.* **77**(2) (1993) 249–254.
7. J. W. Pearson, *Computation of Hypergeometric Functions* (University of Oxford, 2009).
8. M. Carley, Series expansion for the sound field of rotating sources, *J. Acoust. Soc. Am.* **120**(3) (2006) 1252–1256.
9. M. J. Carley, Series expansion for the sound field of a ring source, *J. Acoust. Soc. Am.* **128**(6) (2010) 3375–3380.
10. J. P. Arenas, Numerical computation of the sound radiation from a planar baffled vibrating surface, *J. Comput. Acoust.* **16**(3) (2008) 321–341.
11. M. Abramowitz and I. A. Stegun, *Handbook of Mathematical Functions with Formulas, Graphs and Mathematical Tables* (National Bureau of Standards, Washington, DC, 1972).
12. J. K. Bloomfield, S. H. Face and Z. Moss, Indefinite integrals of spherical Bessel functions, arXiv:1703.06428.
13. M. Červenka and M. Bednařík, On the structure of multi-Gaussian beam expansion coefficients, *Acta Acust. united Ac.* **101**(1) (2015) 15–23.
14. R. M. Aarts and A. J. Janssen, On-axis and far-field sound radiation from resilient flat and dome-shaped radiators, *J. Acoust. Soc. Am.* **125**(3) (2009) 1444–1455.
15. T. Mellow, On the sound field of a resilient disk in free space, *J. Acoust. Soc. Am.* **123**(4) (2008) 1880–1891.
16. V. Mangulis, Acoustic radiation from a wobbling piston, *J. Acoust. Soc. Am.* **40**(2) (1966) 349–353.
17. ISO 9613-1:1993. Acoustics — Attenuation of sound during propagation outdoors — Part 1: Calculation of the absorption of sound by the atmosphere (International Organization for Standardization, Genève, 1993).
18. S. Zhang and J. Jin, *Computation of Special Functions* (John Wiley & Sons, New York, 1996).
19. T. Mellow and L. Kärkkäinen, Comparison of spheroidal and eigenfunction-expansion trial functions for a membrane in an infinite baffle, *J. Acoust. Soc. Am.* **123**(5) (2008) 2598–2602.
20. M. Greenspan, Piston radiator: Some extensions of the theory, *J. Acoust. Soc. Am.* **65**(3) (1979) 608–621.

Appendix A

A.1. *A baffled circular piston with arbitrary axisymmetric velocity profiles*

For a baffled circular piston with an arbitrary axisymmetric velocity profile, Eq. (1) is rewritten as

$$p(\mathbf{r}) = -2\mathrm{j}\rho_0\omega \int_0^{2\pi}\int_0^a V(\rho_\mathrm{s})g(\mathbf{r}_\mathrm{s};\mathbf{r})\ \rho_\mathrm{s}\mathrm{d}\rho_\mathrm{s}\mathrm{d}\varphi_\mathrm{s}, \tag{A.1}$$

where $V(\rho_\mathrm{s})$ is the given surface velocity profile and equals to v_0 for a rigid piston.

The Green function $g(\mathbf{r}_\mathrm{s};\mathbf{r}) = \mathrm{e}^{\mathrm{j}k|\mathbf{r}-\mathbf{r}_\mathrm{s}|}/(4\pi|\mathbf{r}-\mathbf{r}_\mathrm{s}|)$ in Eq. (A.1) can be expanded under the spherical coordinate system as the summation of spherical harmonics

$$\begin{aligned} g(\mathbf{r}_\mathrm{s};\mathbf{r}) = \frac{\mathrm{j}k}{4\pi}\sum_{n=0}^{\infty}(2n+1)\mathrm{h}_n(kr)\mathrm{j}_n(kr_\mathrm{s})\sum_{m=-n}^{n}\frac{(n-m)!}{(n+m)!}\mathrm{P}_n^m(\cos\theta) \\ \times \mathrm{P}_n^m(\cos\theta_\mathrm{s})\mathrm{e}^{\mathrm{j}m(\varphi-\varphi_\mathrm{s})},\ r > r_\mathrm{s}, \end{aligned} \tag{A.2}$$

where $\mathrm{P}_n^m(\cdot)$ is the associated Legendre function at the degree n and order m, and $\theta_\mathrm{s} = \pi/2$ since $z_\mathrm{s} = 0$ for all source points.

Substituting Eq. (A.2) into Eq. (A.1) yields

$$\begin{aligned} p(\mathbf{r}) = \frac{\rho_0 c_0}{2\pi}\sum_{\nu=0}^{\infty}(2n+1)\mathrm{h}_n(kr)\left[\int_0^a \mathrm{j}_n(k\rho_\mathrm{s})V(\rho_\mathrm{s})k^2\rho_\mathrm{s}\mathrm{d}\rho_\mathrm{s}\right] \\ \times \sum_{m=-n}^{n}\frac{(n-m)!}{(n+m)!}\mathrm{P}_n^m(\cos\theta)\mathrm{P}_n^m(\cos\theta_\mathrm{s})\left[\int_0^{2\pi}\mathrm{e}^{\mathrm{j}m(\varphi-\varphi_\mathrm{s})}\mathrm{d}\varphi_\mathrm{s}\right], \end{aligned} \tag{A.3}$$

where the relation $r_\mathrm{s} = \rho_\mathrm{s}$ has been used since $\theta_\mathrm{s} = \pi/2$. Using the substitution $\xi = k\rho_\mathrm{s}$ and performing the integral with respect to φ_s yield

$$p(\mathbf{r}) = \rho_0 c_0\sum_{n=0}^{\infty}(2n+1)\mathrm{P}_n(\cos\theta)\mathrm{P}_n(\cos\theta_\mathrm{s})\mathrm{h}_n(kr)\left[\int_0^{ka} V\left(\frac{\xi}{k}\right)\mathrm{j}_n(\xi)\xi\mathrm{d}\xi\right], \tag{A.4}$$

where all the terms $m > 0$ are eliminated because the integrations are zero. According to the condition $\theta_\mathrm{s} = \pi/2$ and the explicit expression of $\mathrm{P}_n(0)$ (Eq. (4.2.4) in Ref. 18)

$$\mathrm{P}_n(0) = \begin{cases} (-1)^{n/2}\dfrac{\Gamma\left(\dfrac{n}{2}+\dfrac{1}{2}\right)}{\sqrt{\pi}\Gamma\left(\dfrac{n}{2}+1\right)}, & n = \text{ even} \\ 0, & n = \text{odd} \end{cases} \tag{A.5}$$

All the terms in Eq. (A.4) are zero when n is odd and can be omitted. After replacing n by $2n$ and using Eq. (A.5) and Eq. (A.4) can be simplified as

$$p(\mathbf{r}) = \rho_0 c_0 \sum_{n=0}^{\infty} (-1)^n \frac{(4n+1)\Gamma\left(n+\frac{1}{2}\right)}{\sqrt{\pi}\Gamma(n+1)} \mathrm{P}_{2n}(\cos\theta)\mathrm{h}_{2n}(kr)\left[\int_0^{ka} V\left(\frac{\xi}{k}\right)\xi \mathrm{j}_{2n}(\xi)\mathrm{d}\xi\right], \tag{A.6}$$

where $V(\rho_\mathrm{s}) = v_0$ corresponds to Eq. (2).

The integral of spherical Bessel functions is required in Eq. (A.6) and depends on specific surface velocity profiles. For arbitrary axisymmetric distributions, they can be represented as series in different ways with even degrees of (ρ_s/a),[14,19,20] and the following one is adopted in this paper.[13]

$$V(\rho_\mathrm{s}) = v_0 \sum_{m=0}^{\infty} A_m \left(\frac{\rho_\mathrm{s}}{a}\right)^{2m}, \tag{A.7}$$

where A_m are known expansion coefficients. For example, the case $A_0 = 1$ and $A_1 = A_2 = \cdots = 0$ represents a rigid circular piston, the case $A_0 = 2, A_1 = -2$ and $A_2 = A_3 = \cdots = 0$ represents a simply supported disk, and the case $A_0 = 3, A_1 = -6, A_2 = 3$ and $A_3 = A_4 = \cdots = 0$ represents a clamped disk.[14] Substituting Eq. (A.7) into Eq. (A.6) yields the integrals with the form

$$\int_0^{ka} \xi^{2m+1}\mathrm{j}_{2n}(\xi)\mathrm{d}\xi, \ n, m, = 0, 1, 2, \ldots. \tag{A.8}$$

According to the auxiliary indefinite integral Eq. (6) and the recurrence relation Eq. (7), the recurrence steps for the calculation of $\Phi_{2n}^{2m+1}(x)$ are

$$\begin{cases} \Phi_{2n}^{2m+1}(x) = 2(n+m)\Phi_{2n-1}^{2m}(x) - x^{2m+1}\mathrm{j}_{2n-1}(x), \ l = 0 \\ \Phi_{2n-1}^{2m}(x) = 2(n+m-1)\Phi_{2n-2}^{2m-1}(x) - x^{2m}\mathrm{j}_{2n-2}(x), \ l = 1 \\ \quad \vdots \qquad\qquad \vdots \qquad\qquad \vdots \\ \Phi_{2n-l}^{2m+1-l}(x) = 2(n+m-l)\Phi_{2n-l-1}^{2m-l}(x) - x^{2m+1-l}\mathrm{j}_{2n-l-1}(x), \ l \\ \quad \vdots \qquad\qquad \vdots \qquad\qquad \vdots \\ \Phi_{n-m+1}^{m-n+2}(x) = 2\Phi_{n-m}^{m-n+1}(x) - x^{m-n+2}\mathrm{j}_{n-m}(x), \ l = n+m-1 \\ \Phi_{n-m}^{m-n+1}(x) = 0 \times \Phi_{n-m-1}^{m-n}(x) - x^{m-n+1}\mathrm{j}_{n-m-1}(x), \ l = n+m, \end{cases} \tag{A.9}$$

which is equal to Eq. (8) in the paper when $m = 0$ and stop when $l = n + m$ because the coefficient of $\Phi_{n-m-1}^{m-n}(x)$ becomes 0. From the above relationships, $\Phi_{2n}^{2m+1}(x)$ can be represented as Eq. (10).

A.2. *An unbaffled resilient disk with arbitrary axisymmetric pressure profiles*

The sound pressure radiated by a resilient disk in free space (without a baffled) is calculated with the dipole integral.[3,15]

$$p(\mathbf{r}) = \int_0^{2\pi}\int_0^a \mathrm{P}(\rho_\mathrm{s})\left.\frac{\partial g(\mathbf{r}_\mathrm{s};\mathbf{r})}{\partial z_\mathrm{s}}\right|_{z_\mathrm{s}=0}\rho_\mathrm{s}\mathrm{d}\rho_\mathrm{s}\mathrm{d}\varphi_\mathrm{s}, \tag{A.10}$$

where $P(\rho_\mathrm{s})$ is the given pressure profile. The partial derivative in Eq. (A.10) can be transformed into

$$\frac{\partial}{\partial z_\mathrm{s}} = \mathbf{e}_{z_\mathrm{s}}\cdot\nabla_\mathrm{s} = \cos\theta_\mathrm{s}\frac{\partial}{\partial r_\mathrm{s}} - \frac{\sin\theta_\mathrm{s}}{r_\mathrm{s}}\frac{\partial}{\partial\theta_\mathrm{s}}, \tag{A.11}$$

where ∇_s is the gradient operator under the rectangular coordinate system $(x_\mathrm{s}, y_\mathrm{s}, z_\mathrm{s})$ and $\mathbf{e}_{z_\mathrm{s}}$ is the unit vector in the direction of $+z_\mathrm{s}$-axis. By using Eq. (A.11) and the condition $\theta_\mathrm{s} = \pi/2$, the partial derivative of Green function in Eq. (A.10) becomes

$$\begin{aligned}\left.\frac{\partial g(\mathbf{r}_\mathrm{s};\mathbf{r})}{\partial z_\mathrm{s}}\right|_{z_\mathrm{s}=0} &= \left.\left[\cos\theta_\mathrm{s}\frac{\partial g(\mathbf{r}_\mathrm{s};\mathbf{r})}{\partial r_\mathrm{s}} - \frac{\sin\theta_\mathrm{s}}{r_\mathrm{s}}\frac{\partial g(\mathbf{r}_\mathrm{s};\mathbf{r})}{\partial\theta_\mathrm{s}}\right]\right|_{\theta_\mathrm{s}=\pi/2}\\ &= -\left.\frac{\sin\theta_\mathrm{s}}{r_\mathrm{s}}\frac{\partial g(\mathbf{r}_\mathrm{s};\mathbf{r})}{\partial\theta_\mathrm{s}}\right|_{\theta_\mathrm{s}=\pi/2},\end{aligned} \tag{A.12}$$

where the first term is omitted because $\cos\theta_\mathrm{s} = 0$.

Using the spherical expansion of $g(\mathbf{r}_\mathrm{s};\mathbf{r})$ in Eqs. (A.2), (A.12) and (A.10) is expanded as

$$\begin{aligned}p(\mathbf{r}) = \frac{\mathrm{j}}{4\pi}\sum_{n=0}^{\infty}(2n+1)\mathrm{h}_n(\mathrm{kr})\left[\int_0^a P(\rho_\mathrm{s})\mathrm{j}_n(k\rho_\mathrm{s})k\mathrm{d}\rho_\mathrm{s}\right]\sum_{m=-n}^{n}\frac{(n-m)!}{(n+m)!}\\ \times\mathrm{P}_n^m(\cos\theta)\left.\frac{\mathrm{d}\,\mathrm{P}_n^m(\cos\theta_\mathrm{s})}{\mathrm{d}\,\cos\theta_\mathrm{s}}\right|_{\theta_\mathrm{s}=\pi/2}\left[\int_0^{2\pi}\mathrm{e}^{\mathrm{j}m(\varphi-\varphi_\mathrm{s})}\mathrm{d}\varphi_\mathrm{s}\right].\end{aligned} \tag{A.13}$$

Similar to Eq. (A.3), substituting $\xi = k\rho_\mathrm{s}$ and performing the integral with respect to φ_s yield

$$p(\mathbf{r}) = \frac{j}{2}\sum_{n=0}^{\infty}(2n+1)\mathrm{h}_n(kr)\mathrm{P}_n(\cos\theta)\left.\frac{\mathrm{d}\,\mathrm{P}_n(\cos\theta_\mathrm{s})}{\mathrm{d}\,\cos\theta_\mathrm{s}}\right|_{\theta_\mathrm{s}=\pi/2}\left[\int_0^{ka}P\left(\frac{\xi}{k}\right)\mathrm{j}_n(\xi)\mathrm{d}\xi\right]. \tag{A.14}$$

According to the condition $\theta_\mathrm{s} = \pi/2$ and the explicit expression (Eq. (4.2.5) in Ref. 18)

$$\left.\frac{\mathrm{dP}_n(x)}{\mathrm{d}x}\right|_{x=0} = \begin{cases}0, & n = \text{even}\\ \dfrac{2(-1)^{(n-1)/2}}{\sqrt{\pi}}\dfrac{\Gamma\left(\dfrac{n}{2}+1\right)}{\Gamma\left(\dfrac{n}{2}+\dfrac{1}{2}\right)}, & n = \text{odd},\end{cases} \tag{A.15}$$

all the terms in Eq. (A.14) are zero when n is even and can be omitted. After replacing n by $2n+1$ and using Eqs. (A.15) and (A.14) can be simplified as

$$p(\mathbf{r}) = \mathrm{j}\sum_{n=0}^{\infty}(-1)^n \frac{(4n+3)\Gamma\left(n+\frac{3}{2}\right)}{\sqrt{\pi}\Gamma(n+1)} \mathrm{P}_{2n+1}(\cos\theta)\mathrm{h}_{2n+1}(kr)\left[\int_0^{ka}\mathrm{P}\left(\frac{\xi}{k}\right)\mathrm{j}_{2n+1}(\xi)\mathrm{d}\xi\right]. \tag{A.16}$$

The integral of spherical Bessel functions is required in Eq. (A.16) and depends on specific surface pressure profiles. For arbitrary axisymmetric distributions, they can be represented with.[15,19]

$$P(\rho_\mathrm{s}) = p_0\sum_{m=0}^{\infty} B_m\left(\frac{\rho_\mathrm{s}}{a}\right)^{2m}, \tag{A.17}$$

where B_m are known expansion coefficients. For example, the case $B_0 = 1$ and $B_1 = B_2 = \cdots = 0$ represents the disk in free space excited by a uniform pressure.[3] Substituting Eq. (A.17) into Eq. (A.16) yields the integrals with the form

$$\int_0^{ka}\xi^{2m}\mathrm{j}_{2n+1}(\xi)\mathrm{d}\xi, n, m = 0, 1, 2, \ldots. \tag{A.18}$$

Similar to Eq. (A.9), $\Phi_{2n+1}^{2m}(x) = \int x^{2m}\mathrm{j}_{2n+1}(x)\mathrm{d}x$ can be written in closed form as in Eq. (11).

A.3. *A baffled wobbling piston*

The surface velocity profile representing the wobbling effects is $v_0\rho_\mathrm{s}a^{-1}\cos(\varphi_\mathrm{s})$.[16] Similar to the derivations above, the sound pressure can be expanded by using the spherical harmonics Eq. (A.2) as

$$p_\mathrm{w}(\mathbf{r}) = \frac{\rho_0 c_0 v_0}{2\pi ka}\sum_{n=0}^{\infty}(2n+1)\mathrm{h}_n(kr)\left[\int_0^{ka}\xi^2\mathrm{j}_n(\xi)\mathrm{d}\xi\right]\sum_{m=-n}^{n}\frac{(n-m)!}{(n+m)!}\mathrm{P}_n^m(\cos\theta)$$
$$\times\mathrm{P}_n^m(\cos\theta_\mathrm{s})\left[\int_0^{2\pi}\cos\varphi_\mathrm{s}\mathrm{e}^{\mathrm{j}m(\varphi-\varphi_\mathrm{s})}\mathrm{d}\varphi_\mathrm{s}\right]. \tag{A.19}$$

The integral with respect to φ_s in Eq. (A.19) is nonzero only when $m = \pm 1$ because

$$\int_0^{2\pi}\cos\varphi_\mathrm{s}\mathrm{e}^{-\mathrm{j}m\varphi_\mathrm{s}}\mathrm{d}\varphi_\mathrm{s} = \begin{cases}\pi, & m = -1, 1\\ 0, & \text{otherwise}\end{cases}. \tag{A.20}$$

Equation (A.19) is then simplified as

$$p_\mathrm{w}(\mathbf{r}) = \frac{\rho_0 c_0 v_0}{ka}\cos\varphi\sum_{n=0}^{\infty}(2n+1)\mathrm{h}_n(kr)\frac{(n-1)!}{(n+1)!}\mathrm{P}_n^1(\cos\theta)\mathrm{P}_n^1(\cos\theta_\mathrm{s})\left[\int_0^{ka}\xi^2\mathrm{j}_n(\xi)\mathrm{d}\xi\right]. \tag{A.21}$$

According to the relation $\theta_{\mathrm{s}} = \pi/2$ and Eq. (4.4.3) in Ref. 18

$$\mathrm{P}_n^1(0) = \begin{cases} 0, & n = \text{even} \\ (-1)^{\frac{n+1}{2}} \dfrac{2}{\sqrt{\pi}} \dfrac{\Gamma\left(\dfrac{n}{2}+1\right)}{\Gamma\left(\dfrac{n}{2}+\dfrac{1}{2}\right)}, & n = \text{odd} \end{cases}. \tag{A.22}$$

All the terms in Eq. (A.22) are zero when n is even and can be omitted. After replacing n by $2n+1$ and using Eqs. (A.22) and (A.21) can be simplified as Eq. (12) in this paper.

The directivity factor of the wobbling effects is given by Eq. (6) in Ref. 16 as

$$D_{\mathrm{w}}(\theta, \varphi) = -2\mathrm{j} \cos\varphi \frac{\mathrm{J}_2(ka \sin\theta)}{ka \sin\theta}, \tag{A.23}$$

where $\mathrm{J}_2(\cdot)$ is the Bessel function at order 2. To obtain the directivity factor of the proposed solution, the approximation $\mathrm{h}_{2n+1}(kr) \sim \mathrm{j}(-1)^{n+1}\mathrm{h}_0\,(kr)$ at $kr \to \infty$ is substituted into the sound pressure expression Eq. (12), yielding

$$\begin{aligned} p_{\mathrm{w}}(\theta, \varphi) = {} & \frac{\rho_0 c_0 v_0}{(ka)(kr)} \mathrm{e}^{\mathrm{j}kr} \cos\varphi \sum_{n=0}^{\infty} \frac{(4n+3)\Gamma\left(n+\dfrac{3}{2}\right)}{\sqrt{\pi}(2n+1)\Gamma(n+2)} \mathrm{P}_{2n+1}^1(\cos\theta) \\ & \times \left[\int_0^{ka} \xi^2 \mathrm{j}_{2n+1}(\xi)\mathrm{d}\xi\right], \end{aligned} \tag{A.24}$$

where the integral $\int_0^{ka} \xi^2 \mathrm{j}_{2n+1}(\xi)\mathrm{d}\xi$ can be calculated with Eq. (11). To obtain the directivity factor, Eq. (A.24) needs to be normalized by

$$D_0 = \frac{-\mathrm{j}\rho_0 c_0 v_0 ka^2}{2r} \mathrm{e}^{\mathrm{j}kr}, \tag{A.25}$$

which is obtained by letting $\theta = 0$ for the case of the radiation from a baffled rigid piston. Dividing Eq. (A.24) by Eq. (A.25) yields

$$D_{\mathrm{w}}(\theta, \varphi) = \frac{2\mathrm{j}}{(ka)^3} \cos\varphi \sum_{n=0}^{\infty} \frac{(4n+3)\Gamma\left(n+\dfrac{3}{2}\right)}{\sqrt{\pi}(2n+1)\Gamma(n+2)} \mathrm{P}_{2n+1}^1(\cos\theta) \left[\int_0^{ka} \xi^2 \mathrm{j}_{2n+1}(\xi)\mathrm{d}\xi\right]. \tag{A.26}$$

It can be demonstrated by numerical calculations (not presented here for simplicity) that Eq. (A.26) is identical to Eq. (A.23).